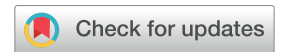
## **ChemComm**



### COMMUNICATION

View Article Online
View Journal | View Issue



Cite this: *Chem. Commun.*, 2019, 55, 5619

Received 2nd March 2019, Accepted 17th April 2019

DOI: 10.1039/c9cc01725a

rsc.li/chemcomm

# Single-crystal-to-single-crystal guest exchange in columnar assembled brominated triphenylamine bis-urea macrocycles†

Ammon J. Sindt,<sup>a</sup> Mark D. Smith, <sup>b</sup> Samuel Berens,<sup>b</sup> Sergey Vasenkov, <sup>b</sup> Clifford R. Bowers<sup>c</sup> and Linda S. Shimizu <sup>b</sup>\*

Self-assembly of brominated triphenylamine bis-urea macrocycles affords robust porous materials. Urea hydrogen bonds organize these building blocks into 1-dimensional columns, which pack *via* halogen—aryl interactions. The crystals are stable when emptied, present two distinct absorption sites for Xe with restricted Xe diffusion, and exhibit single-crystal-to-single-crystal guest exchange.

Porous materials are advantageous for catalysis, <sup>1</sup> as nanoreactors, <sup>2</sup> and for the confinement of photo-luminescent compounds<sup>3</sup> as well as for storage, <sup>4</sup> sensing, <sup>5</sup> and separations <sup>6</sup> of small molecules. Key to these processes is how the host and guest influence and interact with each other to afford synergetic properties. Single-crystal-to-single-crystal (SC–SC) transformations can follow these molecular processes by providing atomic details to elucidate the factors that guide the molecular interactions. SC–SC transformations can be triggered under a number of conditions including: temperature, <sup>7</sup> photo-irradiation, <sup>8</sup> guest inclusion, <sup>9</sup> pressure, <sup>10</sup> and mechanoresponses. <sup>11</sup> Here, we investigate SC–SC guest exchange in porous organic crystals of triphenylamine bis-urea macrocycles.

Typically, hosts for these studies are assembled from rigid materials. Examples include metal organic frameworks (MOFs), 12 hydrogen bonded organic frameworks (HOFs), 3 and porous organic materials. 14 The latter can be beneficial due to the structural versatility organic molecules provide and the ease of forming porous materials simply through crystallization. However, it can be challenging to predict how molecules will assemble in the solid-state. Close-packing principles are often at odds with forming permeable materials. Therefore, molecular families that reliably form porous materials upon crystallization are highly sought after since they offer tunability within their host framework. 15 The Shimizu group employs simple bis-urea building blocks that stack

into pillars and columns to form nanoporous molecular crystals

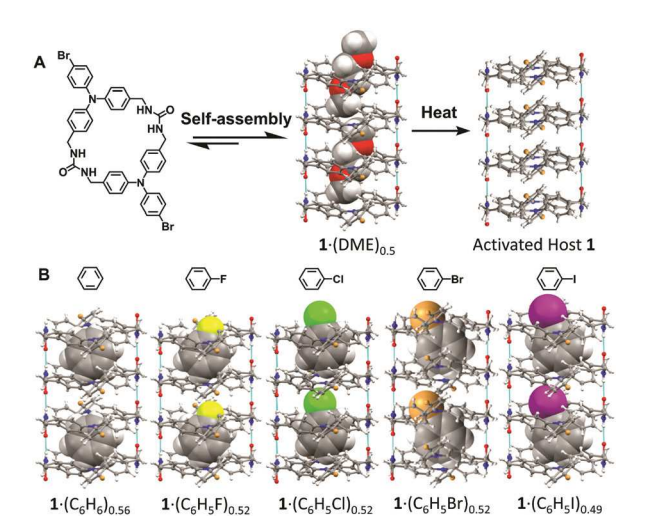


Fig. 1 (A) Self-assembly of macrocycle 1 from the vapour diffusion of DME into DMSO leads to 1D channels. Subsequent heating activates the channels for the loading of different guests. (B) SC-SC transformations observed upon soaking activated host 1 crystals in guest liquids.

that can be used as containers for photochemical reactions. 16 While experimental evidence suggests these frameworks remain intact during the process of guest exchange and subsequent photoreactions, this is our first demonstration of SC-SC transformations. We report a porous organic material made from a triphenylamine (TPA) bis-urea macrocycle 1, which contains two bromo-TPA units (Fig. 1). This macrocycle crystallizes into columnar structures through urea-urea interactions with columns packing together with  $\pi$ - $\pi$  and halogen- $\pi$  interactions forming large crystals  $(35 \times 265 \,\mu\text{m})$  that are robust and suitable for SC transformations. Simple heating removes the guest affording homogeneous nanochannels. Immersion of the material into an organic solvent results in a SC-SC transformation to afford a new host:guest complex (Fig. 1B). These complexes organize guests near photoactive TPA units and should consequently enable us to study the effects of closely oriented guests on the optoelectronic properties.

<sup>&</sup>lt;sup>a</sup> Department of Chemistry and Biochemistry, University of South Carolina, Columbia, SC 29208, USA. E-mail: SHIMIZLS@mailbox.sc.edu

<sup>&</sup>lt;sup>b</sup> Department of Chemical Engineering, University of Florida, Gainesville, FL 32611, USA

<sup>&</sup>lt;sup>c</sup> Department of Chemistry, University of Florida, Gainesville, FL 32611, USA

 $<sup>\</sup>dagger$  Electronic supplementary information (ESI) available: Experimental details and synthesis/characterization of compounds. CCDC 1899526–1899533. For ESI and crystallographic data in CIF or other electronic format see DOI: 10.1039/c9cc01725a

Communication ChemComm

Macrocycle 1 was synthesized by a strategy similar to its linear counterpart. 17 First, commercial bromotriphenylamine was converted to the dialdehyde using a Vilsmeier-Haack reaction followed by hydride reduction resulting in the diol. Once the alcohols were brominated, two TPA units were connected with two triazinanone spacers under basic conditions, resulting in the protected macrocycle. These macrocycles crystallized in chloroform solutions as colourless blocks as a 1:8 macrocycle: CHCl<sub>3</sub> solvate, enabling their purification (Fig. S9, ESI†). Subsequent urea deprotection with diethanolamine under acidic conditions afforded 1 as a beige powder.

Vapour diffusion of 1,2-dimethoxyethane (DME) into a dimethylsulfoxide (DMSO) solution of 1 ( $\sim 2.5$  mg mL<sup>-1</sup>) produced large colourless needles  $(0.6 \times 0.08 \times 0.04 \text{ mm}^3)$  crystallizing in the space group  $P2_1/c$  of the monoclinic system. In this structure, the macrocycle adopts an anti-conformation with encapsulated, disordered DME solvent in a 2:1 ratio (Fig. 2A). Both the macrocycle and DME solvent were found on crystallographic inversion centres with the solvent being situated across an additional inversion centre leading to its disorder within the channels. Individual macrocycles assemble into columnar structures organized by the characteristic threecentred urea hydrogen bond, with  $N(H) \cdot \cdot \cdot O$  distances of 2.848(4) and 2.929(4) Å. This creates infinite hydrogen bonded tubes along the crystallographic b axis with a macrocycle to macrocycle repeat distance of 4.620(2) Å.  $\pi$ -stacking between neighbouring TPAs provides additional stabilization within the columns (Fig. S17, ESI†).

Individual columns assemble into pseudo-hexagonal rodpacking arrays, similar to other bis-urea structures. However, crystals of 1 are on average ten times larger in width (35  $\times$ 265  $\mu m$  versus 3  $\times$  250  $\mu m$  , Fig. S10, ESI†) than any other previously obtained bis-urea macrocycle derivative. 16 Hirshfeld analysis was used to identify key interactions that guide assembly and subsequent packing of the columns of 1 to facilitate the growth of larger crystals. 18 Fig. 2B and C shows the  $d_{\text{norm}}$  surface and highlights the key urea motif driving individual column formation as well as close intercolumnar contacts occurring between the bromine substituents and aryl rings. The halogen- $\pi$  interactions illustrated in Fig. 2C display a Br···Caryl distance of 3.303(3) Å, which is shorter the sum of the vdW radii (3.5 Å) suggesting that the

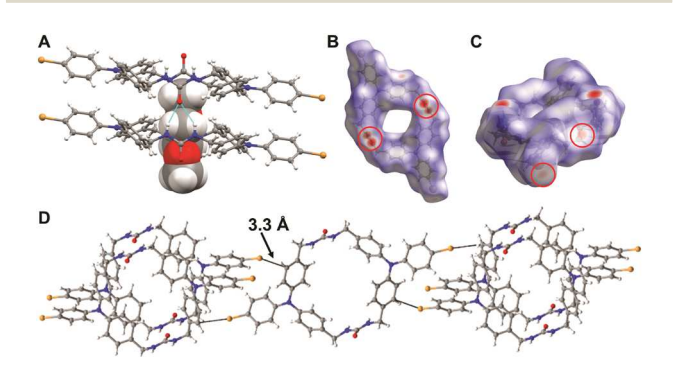


Fig. 2 (A) View along a single column illustrating the 2:1 host: guest ratio and the three-centred urea hydrogen bonding motif. (B)  $d_{\mathrm{norm}}$  surface showing urea interactions (circled in red). (C)  $d_{\rm norm}$  surface showing halogen $-\pi$  interactions (circled in red). (D) Crystal packing showing select close contacts between columns.

p-bromophenyl groups significantly increases intercolumnar interactions in 1 versus the more cylindrical bis-urea macrocycles. 19

Fig. 3 compares a series of bis-urea macrocycles that assembled into similar 1-dimensional columns. Host 1, phenyl ether (2), and benzophenone (3) have similar cavity sizes and topographies (Table S3, ESI†). The cavities are roughly elliptical, displaying cross sectional diameters of  $\sim 4$  Å  $\times$  7 Å (Fig. 3A). The walls of these channels are held together by urea hydrogen bonds, with further stabilization coming from aryl stacking interactions. In 2 and 3, these are edge-to-face  $\pi$ -stacking interactions while the extra phenyl groups in 1 lead to offset  $\pi$ -stacking. The alternative edge-to-face aryl stacking interactions in 2 and 3 give the channels a curvature highlighted in blue in Fig. 3B, which oscillates back and forth along the length of the columns. These oscillations are also pronounced in the offset-aryl stacked structure of host 1. The channels of hosts 2 proved to be an ideal substrate for monitoring single file diffusion of xenon.20 Therefore, we sought to test if the framework of 1 was stable in the absence of guests to see if it could be used for a similar application.

To monitor guest removal, thermogravimetric analysis (TGA) was applied. Host 1.DME crystals displayed a one-step desorption curve with a weight loss of 5.3% between 0 and 90° (Fig. S18, ESI†). Higher temperatures (>90 °C) caused degradation of the material, which was readily detected by NMR. From the percent weight loss, we calculated the macrocycle: guest stoichiometry as 1:0.5. On average a host: guest ratio of 1:0.55 was found over three batches of crystals. The larger crystal size and heavy bromine atoms in 1 facilitated rapid monitoring of the empty host framework by SC-XRD. To ascertain if the host framework would be maintained, one freshly activated crystal was examined immediately after TGA completion and a second crystal after three days on the lab bench in ambient air. Remarkably, the structures, including the columnar framework and packing, were nearly identical to the 1-DME crystals except that the electron density of the DME was absent (Fig. 1A, activated host). The largest electron density maxima found inside the channels within either data set was 0.21  $e^{-}/Å^{3}$ ,

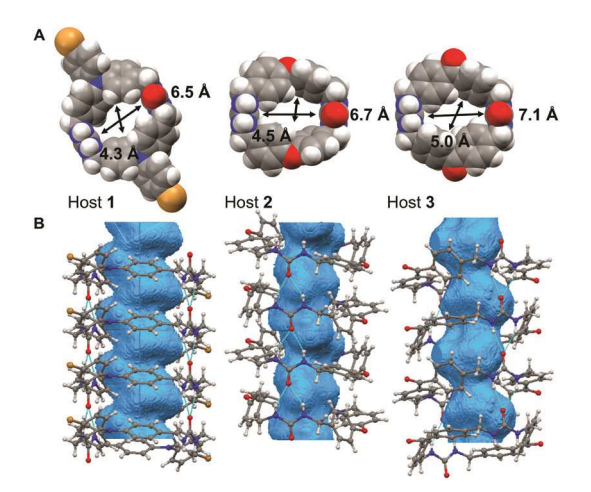


Fig. 3 (A) Pore sizes of different bis-urea macrocycles subtracting the vdW radii. From left to right the urea spacers are 4-bromotriphenylamine, phenyl ether, and benzophenone. (B) Comparison of their corresponding 1-dimensional columns of 1-3 with their void space highlighted in blue.

ChemComm Communication

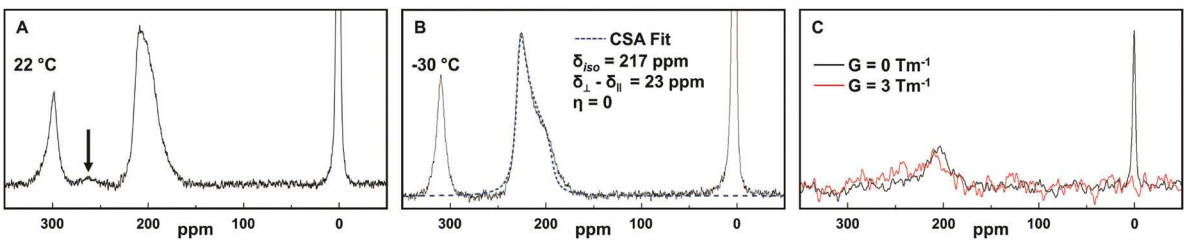


Fig. 4 129Xe NMR spectra of 1 acquired at 138.45 MHz (11.756 T) at (A) 295 K and (B) 243 K by accumulating 1920 and 960 transients respectively, with a recycle delay of  $40 \times$  and pulse length of  $10 \mu s$ . The dashed blue trace is the least-squares fit<sup>24</sup> to an axially symmetric chemical shift anisotropy powder pattern. (C) <sup>129</sup>Xe NMR spectra measured using a stimulated echo PFG NMR sequence at 298 K and diffusion time 5 ms.

i.e. essentially background noise (see ESI†). These results demonstrate the stability of this assembled material under ambient conditions in the absence of guests.

To further characterize the pore space architecture of host 1, freshly evacuated crystals were pressurized to 9.5 bar (at 298 K) with isotopically enriched Xe gas and examined by <sup>129</sup>Xe NMR. <sup>129</sup>Xe NMR has previously been used to study 1D channels<sup>21</sup> since the <sup>129</sup>Xe NMR chemical shift tensor is highly sensitive to the pore-space structure and shows dependence on de-shielding due to Xe-Xe interactions, especially at higher Xe loadings in single-file nanotubular pores, where cross-sectional dimensions are comparable to the vdW diameter of the Xe atom (0.44 nm). 22,23 Fig. 4A and B show the NMR spectra for <sup>129</sup>Xe·1 at 295 and 243 K referenced to gas phase 129Xe at 0 ppm. A well-defined axially symmetric chemical shift anisotropy (CSA) powder pattern with  $\delta_{\rm iso}$  = 217 ppm emerges upon cooling the sample to 243 K. This <sup>129</sup>Xe CSA tensor is consistent with a high Xe loading in channels with the dimensions of host  $\mathbf{1}$ . The symmetric peak centered near 310 ppm is attributed to highly confined Xe atoms residing in pores with (dynamically averaged) cubic symmetry in host 1, tentatively identified as the inter-columnar pores (Fig. S20, ESI†). The ratio of the areas of the adsorbed Xe peaks are close to 3:1 at both temperatures. In the spectrum recorded at 295 K, the small peak that appears near 260 ppm (indicated by the arrow in Fig. 4A) suggests that Xe is in fast chemical exchange between the two types

<sup>129</sup>Xe PFG NMR experiments were performed at 298 K to investigate the diffusion of Xe atoms adsorbed inside the 1-D channels. Unfortunately, short  $T_2$  NMR relaxation times (see ESI†) prevented us from using sufficiently large gradient pulse durations and amplitudes to measure intra-channel diffusion. However, these diffusion studies allowed us to qualitatively examine the exchange of Xe atoms between the channels and the surrounding gas phase on the time scale of the diffusion observation (5-100 ms). It was found that a complete diffusion attenuation of the gas-phase line could be achieved with an expected gas-phase diffusivity of  $6.7 \times 10^{-7} \text{ m}^2 \text{ s}^{-1}$  at 298 K. However, there was no noticeable diffusion attenuation of the line corresponding to Xe atoms adsorbed in the channels (Fig. 4C). This was seen for all diffusion times used. The observed lack of the diffusion attenuation for the Xe line at 206 ppm allows us to estimate a lower limit of 100 ms on the exchange time (see ESI†). Therefore, we can conclude that there are no defects in the channel walls that might lead to such an exchange.

To investigate the ability of this host to absorb and store small molecules, we treated the activated crystals with a series of halogenated benzenes. Host 1-DME crystals were consistently activated for SC-SC exchange by heating at 90 °C for  $\sim$  2.5 h until no further weight loss was detected *via* TGA (Fig. S18, ESI†). Freshly activated crystals (5 mg) were then immersed in a liquid guest (1 mL) for 1 day followed by examination with SC-XRD. SC-SC transformations were observed giving five host 1 guest structures that displayed 1:0.5 host guest stoichiometry including 1·C<sub>6</sub>H<sub>6</sub>, 1·C<sub>6</sub>H<sub>5</sub>F, 1·C<sub>6</sub>H<sub>5</sub>Cl, 1·C<sub>6</sub>H<sub>5</sub>Br, and 1·C<sub>6</sub>H<sub>5</sub>I. All the inclusion crystals were found to be isoskeletal with one another, the original DME solvate, and the activated host. Fig. 1B highlights the similarity between these host:guest complexes.

In all cases, the guests showed a moderate amount of disorder within the columns. Fortunately, the halogen-substituted guests permitted more reliable determination despite this disorder due to the larger X-ray scattering factors (especially for Cl, Br and I). The guests aligned in a planar tape-like manner within the channels with guests being crystallographically modelled on two independent sites, one having the halogen-benzene bond more perpendicular to the macrocycle, shown for iodobenzene in Fig. 5A (red structure) with the other in a slightly tilted orientation (Fig. 5A, orange). Both of these sites were located

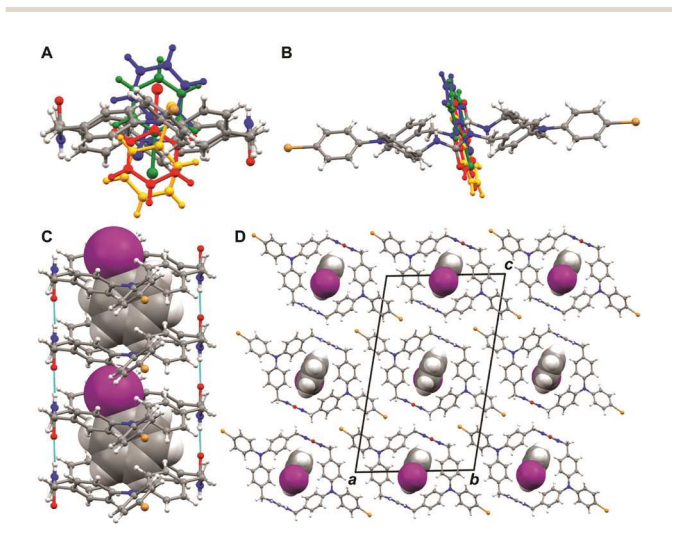


Fig. 5 Crystal views of  $1 \cdot C_6 H_5 I$ . (A) View of disorder of guest inside the host 1. Four sites are found. (B) Another view of guest disorder. (C) Spacefilled guests inside host 1. (D) Crystal packing of host 1 with guests. For (C) and (D), disorder was removed for clarity.

Communication ChemComm

near inversion centres (Fig. 5A, blue and green) giving a total of four possible sites for the guest location, with each having similar occupancies. This disorder was quite similar across all structures. The alignment of the guests in all of these structures may arise from C-H···halogen and/or C-H··· $\pi$  interactions; however, these details are obscured by the crystallographic disorder.

In summary, a brominated TPA bis-urea macrocycle assembled to form robust crystals with accessible columnar channels suitable for SC-SC guest exchange. The host is stable when emptied and exhibits confined 129Xe NMR signals when pressurized under xenon. 129Xe PFG NMR measurements suggest these channels are homogeneous. Most intriguingly, assembly of this macrocycle orients the individual TPAs close in space to potential guests and enforces close contacts between the two units. Since TPAs are known to undergo chemical or electrochemical oxidation to generate radical cations, these crystalline materials offer potential models for the investigation of electron transfer between organic molecules within confinement. Indeed, linear analogues of host 1 showed stable and regenerable radical formation upon UV-irradiation in the solid-state.<sup>17</sup> Currently, we are evaluating guests that can undergo electron transfer with the TPA units and hope to report on these in due time.

This work was supported in part by the National Science Foundation (NSF) CHE-1608874 and OIA-1655740. A portion of this work was performed at the National High Magnetic Field Laboratory's AMRIS Facility, which is supported by NSF Cooperative Agreement No. DMR-1644779 and the State of Florida.

### Conflicts of interest

There are no conflicts to declare.

#### References

- A. Dhakhinamoorthy, M. Alvaro and H. Garcia, *Chem. Commun.*, 2012, **48**, 11275; S.-Y. Ding, J. Gao, Q. Wang, Y. Zhang, W.-G. Song, C.-Y. Su and W. Wang, *J. Am. Chem. Soc.*, 2011, **133**, 19816.
- 2 V. Ramamurthy and J. Sivaguru, Chem. Rev., 2016, 116, 9914.
- 3 G. Tabacchi, ChemPhysChem, 2018, 19, 1249.
- 4 S. Kitagawa, R. Kitaura and S. Noro, *Angew. Chem., Int. Ed.*, 2004, 43, 2334; P. Sozzani, S. Bracco, A. Comotti, L. Ferretti and R. Simonutti, *Angew. Chem., Int. Ed.*, 2005, 44, 1816; C. M. Kane, A. Banisafar, T. P. Dougherty, L. J. Barbour and K. T. Holman, *J. Am. Chem. Soc.*, 2016, 138, 4377.
- 5 L. E. Kreno, K. Leong, O. K. Farha, M. Allendorf, R. P. Van Duyne and J. T. Hupp, *Chem. Rev.*, 2012, 112, 1105; D. J. Wales, J. Grand, V. P. Ting, R. D. Burke, K. J. Edler, C. R. Bowen, S. Mintova and A. D. Burrows, *Chem. Soc. Rev.*, 2015, 44, 4290; M. Mastalerz, *Acc. Chem. Res.*, 2018, 51, 2411.
- 6 K. Sumida, D. L. Rogow, J. A. Mason, T. M. McDonald, E. D. Bloch, Z. R. Herm, T.-H. Bae and J. R. Long, Chem. Rev., 2012, 112, 724;

- J.-R. Li, J. Sculley and H.-C. Zhou, *Chem. Rev.*, 2012, **112**, 869; J. Lü and R. Cao, *Angew. Chem., Int. Ed.*, 2016, **55**, 9474.
- S. Lee, S. Y. Hwang, H. Lee and O.-S. Jung, Cryst. Growth Des., 2018,
   18, 1278; C.-F. Zhuang, J. Zhang, Q. Wang, Z.-H. Chu, D. Fenske and
   C.-Y. Su, Chem. Eur. J., 2009, 15, 7578.
- 8 S.-L. Huang, T. S. A. Hor and G.-X. Jin, Coord. Chem. Rev., 2017, 346, 112; T. Seki, K. Sakurada, M. Muromoto and H. Ito, Chem. Sci., 2015, 6, 1491.
- V. I. Nikolayenko, D. C. Castell, D. P. van Heerden and L. J. Barbour, Angew. Chem., Int. Ed., 2018, 57, 12086; V. I. Nikolayenko, L. M. van Wyk, O. Q. Munro and L. J. Barbour, Chem. Commun., 2018, 54, 6975; E. S. O'Brien, M. T. Trinh, R. L. Kann, J. Chen, G. A. Elbaz, A. Masurkar, T. L. Atallah, M. V. Paley, N. Patel, D. W. Paley, I. Kymissis, A. C. Crowther, A. J. Millis, D. R. Reichman, X.-Y. Zhu and X. Roy, Nat. Chem., 2017, 9, 1170.
- 10 B. A. Zakharov, A. S. Marchuk and E. V. Boldyreva, CrystEngComm, 2015, 17, 8812; B. A. Zakharov and E. V. Boldyreva, Acta Crystallogr., Sect. B: Struct. Sci., Cryst. Eng. Mater., 2013, B69, 271.
- G. Liu, J. Liu, Y. Liu and X. Tao, J. Am. Chem. Soc., 2014, 136, 590;
   M. Jin, T. Sumitani, H. Sato, T. Seki and H. Ito, J. Am. Chem. Soc., 2018, 140, 2875.
- M. Alhamami, H. Doan and C.-H. Cheng, *Materials*, 2014, 7, 3198;
   K. Yan, R. Dubey, T. Arai, Y. Inokuma and M. Fujita, *J. Am. Chem. Soc.*, 2017, 139, 11341.
- 13 H. Wahl, D. A. Haynes and T. Le Roex, Cryst. Growth Des., 2017, 17, 4377; Y. Li, M. Handke, Y.-S. Chen, A. G. Shtukenberg, C. T. Hu and M. D. Ward, J. Am. Chem. Soc., 2018, 140, 12915.
- 14 J. T. A. Jones, D. Holden, T. Mitra, T. Hasell, D. J. Adams, K. E. Jelfs, A. Trewin, D. J. Willock, G. M. Day, J. Bacsa, A. Steiner and A. I. Cooper, *Angew. Chem., Int. Ed.*, 2011, 50, 749; E. Sanna, E. C. Escudero-Adán, A. Bauzá, P. Ballester, A. Frontera, C. Rotger and A. Costa, *Chem. Sci.*, 2015, 6, 5466.
- 15 R. Natarajan, L. Bridgland, A. Sirikulkajorn, J.-H. Lee, M. F. Haddow, G. Magro, B. Ali, S. Narayanan, P. Strickland, J. P. H. Charmant, A. G. Orpen, N. B. McKeown, C. G. Bezzu and A. P. Davis, *J. Am. Chem. Soc.*, 2013, 135, 16912.
- 16 L. S. Shimizu, S. R. Salpage and A. A. Korous, Acc. Chem. Res., 2014, 47, 2116.
- 17 A. J. Sindt, B. A. DeHaven, D. F. McEachern, D. M. M. M. Dissanayake, M. D. Smith, A. K. Vannucci and L. S. Shimizu, Chem. Sci., 2019, 10, 2670.
- F. L. Hirshfeld, Theor. Chim. Acta, 1977, 44, 129; M. A. Spackman and D. Jayatilaka, CrystEngComm, 2009, 11, 19; J. J. McKinnon, D. Jayatilaka and M. A. Spackman, Chem. Commun., 2007, 3814;
   S. K. Wolff, D. J. Grimwood, J. J. McKinnon, M. J. Turner, D. Jayatilaka and M. A. Spackman, CrystalExplorer (Version 3.1), University of Western Australia, 2012.
- L. S. Shimizu, A. D. Hughes, M. D. Smith, M. J. Davis, B. P. Zhang, H.-C. zur Loye and K. D. Shimizu, J. Am. Chem. Soc., 2003, 125, 14972;
   M. B. Dewal, Y. Xu, J. Yang, F. Mohammed, M. D. Smith and L. S. Shimizu, Chem. Commun., 2008, 3909.
- 20 C. R. Bowers, M. Dvoyashkin, S. R. Salpage, C. Akel, H. Bhase, M. F. Geer and L. S. Shimizu, ACS Nano, 2015, 9, 6343.
- 21 P. Sozzani, A. Comotti, T. Meersmann, J. W. Logan and A. Pines, Angew. Chem., Int. Ed., 2000, 39, 2695; D. V. Soldatov, I. L. Moudrakovski, E. V. Grachev and J. A. Ripmeester, J. Am. Chem. Soc., 2006, 128, 6737.
- 22 J.-L. Bonardet, J. Fraissard, A. Gédéon and M.-A. Springuel-Huet, Catal. Rev.: Sci. Eng., 1999, 41, 115; C.-Y. Cheng and C. R. Bowers, ChemPhysChem, 2007, 8, 2077.
- 23 E. Weiland, M.-A. Springuel-Huet, A. Nossov and A. Gédéon, Microporous Mesoporous Mater., 2016, 225, 41.
- 24 D. Massiot, F. Fayon, M. Capron, I. King, S. Le Calvé, B. Alonso, J.-O. Durand, B. Bujoli, Z. Gan and G. Hoatson, *Magn. Reson. Chem.*, 2002, 40, 70.